INTERNATIONAL JOURNAL FOR NUMERICAL METHODS IN FLUIDS
Int. J. Numer. Meth. Fluids 2008; **58**:1–25
Published online 8 December 2007 in Wiley InterScience (www.interscience.wiley.com). DOI: 10.1002/fld.1674

A well-balanced Runge–Kutta discontinuous Galerkin method for the shallow-water equations with flooding and drying

A. Ern, S. Piperno*, † and K. Djadel

CERMICS, École des Ponts, Université Paris-Est, 77455 Marne La Vallée cedex 2, France

SUMMARY

We build and analyze a Runge–Kutta discontinuous Galerkin method to approximate the one- and two-dimensional shallow-water equations. We introduce a flux modification technique to derive a well-balanced scheme preserving steady states at rest with variable ground elevation and a slope modification technique to deal satisfactorily with flooding and drying. Numerical results illustrating the performance of the proposed scheme are presented. Copyright © 2007 John Wiley & Sons, Ltd.

Received 12 June 2007; Revised 5 September 2007; Accepted 20 October 2007

KEY WORDS: Runge–Kutta discontinuous Galerkin; shallow-water equations; source terms; well-balanced schemes; flooding and drying

1. INTRODUCTION

Free-surface water flows occur in many domains of practical importance such as coastal and river engineering, dam break problems, or ocean modeling. In many cases, such flows can be satisfactorily modeled by the so-called *shallow-water equations* (SWE), which are derived by considering the depth-averaged three-dimensional incompressible Navier–Stokes equations, assuming hydrostatic pressure distribution, and neglecting vertical acceleration and viscous effects [1, 2]. The SWE consist of a set of nonlinear first-order partial differential equations of hyperbolic type with source terms (also called balance laws).

The discretization of the SWE has been the subject of extensive literature. Until recent years, the most commonly chosen numerical methods were finite differences (FD), continuous finite elements

*Correspondence to: S. Piperno, CERMICS, École des Ponts, Université Paris-Est, 77455 Marne La Vallée cedex 2, France.
†E-mail: serge.piperno@cermics.enpc.fr

Contract/grant sponsor: Direction de la Recherche et des Affaires Scientifiques et Techniques (DRAST); contract/grant number: 04 DST 6 07

(CFE), and finite volumes (FV). We refer, for instance, to [3, 4] for FD, to [5–7] for CFE and to [4, 8–11] for FV. The main motivation for using FV is that such methods are especially tailored to discretize conservation laws possibly with shocks, usually producing approximate solutions with local conservation properties. The main drawback of first-order FV is their low order of convergence, even in the case of smooth solutions. To avoid this situation, one can enhance the order of the spatial approximation by using slope reconstruction techniques like the MUSCL scheme [12] or WENO reconstructions [13], whereby high-order accuracy can be achieved on structured meshes. Another possibility on both structured and unstructured meshes consists of using higher-order polynomials within mesh elements, leading to so-called discontinuous Galerkin (DG) methods. DG methods approximate the solution in a finite element setting, but in contrast to CFE which use trial and test spaces spanned by continuous piecewise polynomial functions, DG methods use trial and test spaces spanned by piecewise polynomial functions without enforcing explicitly any continuity between adjacent mesh cells. DG methods with polynomial order set to zero can be interpreted as first-order FV schemes.

Since their introduction more than 30 years ago (see [14, 15] for pioneering works), DG methods have experienced a vigorous development. On a given mesh and using a fixed polynomial order, DG methods involve more degrees of freedom than CFE. However, DG methods possess several attractive features, namely they are well suited to *hp*-adaptive procedures, they can be implemented on arbitrary meshes without enforcing geometric conformity, and they are amenable to parallel computation owing in particular to the block-diagonal structure of the mass matrix. Moreover, when approximating conservation laws, DG methods lead to local conservation properties at the cell level, as in FV. We refer to [16, 17] for a general review of DG methods.

Significant progress in the application of DG methods to the SWE has been achieved in the last few years for various applications, such as dam break problems and flows in channels [18–24], harbor wave disturbances and tidal flows [21, 25–27], flooding and drying [22], or geophysical flows [28]. However, two issues relevant in many applications, namely (i) preserving steady states at rest with variable ground elevation and (ii) properly handling flooding and drying, are still under investigation. The main purpose of this work is to design and analyze a DG discretization of the SWE that can satisfactorily handle these two issues.

- *Preserving steady states at rest*: This guarantees that still areas remain still and that small spurious waves are not artificially triggered by differences in the handling of different terms in the SWE. It has been observed that this feature generally yields more accurate approximate solutions [29]. The standard FV and DG schemes for the SWE do not preserve steady states at rest, because this property requires a compatibility between the numerical flux and the approximation of the source term. In the framework of FV, several techniques have been proposed to preserve steady states at rest, leading to so-called *well-balanced schemes*; see [8, 10, 11] where additional terms are included in the flux calculation and [9] where a so-called upwind discretization of the source term is proposed. High-order well-balanced FV (WENO) and DG schemes for a class of balance laws (including the SWE) have been proposed in [30]. In the DG framework, the well-balanced schemes of [30] amount to modifying the noncentered part of the numerical flux and the source term using integration by parts. In the present work, we propose and analyze a *flux modification* technique for DG methods inspired by the *hydrostatic reconstruction* developed for a kinetic scheme in [8], but the schemes derived in [30] can be used as well. A comparison of the present well-balanced scheme and that of [30] will be given later.

DOI: 10.1002/fld

- *Properly handling flooding and drying*: This is also a difficult task, with many applications in coastal and water engineering. One major difficulty when dealing with flooding and drying is to guarantee that the discrete water height remains non-negative. Besides their lack of physical meaning, negative values lead to difficulties in the computation of the numerical fluxes since the wave speed involves the square root of the water height. In the context of first-order FV methods, flooding and drying have been addressed for instance in [31] for steady and in [32] for unsteady flows. Depending on the values taken by the water height and the ground elevation on adjacent cells, the procedure (which preserves mass) can involve a modification of the former or of the latter. In the context of DG methods, very few published papers deal with flooding and drying. Articles by Bokhove and co-workers [22, 23] consider flooding and drying using space–time DG methods. Space–time elements separate accurately the wet and dry subdomains by moving the mesh accordingly in a transient manner. It is still a difficult task to deal with complex topology of the wet and dry subdomains. DG simulations of flows involving dry beds have also been reported recently [33, 34]. In the present work, we introduce a *slope modification* technique based on the idea of threshold usually used in the framework of FV. Moreover, we use the Harten–Lax–van Leer–Einfeldt (HLLE) flux [35] in one space dimension and the Harten–Lax–van Leer–Contact (HLLC) flux [21] in two space dimensions which, contrary to Roe's flux for example, ensure a property of nonnegativity for the approximate water height [36].

This paper is organized as follows. In Section 2, the SWE and the main features of the Runge–Kutta discontinuous Galerkin (RKDG) scheme introduced in [21] to approximate the SWE are restated. In Section 3, the flux modification technique yielding a well-balanced RKDG method is analyzed and compared with the scheme proposed in [30]. In Section 4, the slope modification technique that deals with flooding and drying is described. In Section 5, numerical tests are presented to illustrate the performance of the proposed method. Conclusions are reached in Section 6. For completeness, Appendix A briefly describes the HLLE and the HLLC fluxes.

2. APPROXIMATION OF THE SWE BY RKDG METHODS

This section restates the main features of the classical RKDG scheme introduced in [21] to approximate the SWE. This scheme will serve as the basis for the new developments presented in Sections 3 and 4.

2.1. Governing equations

Let the domain Ω be an open-bounded subset of $\mathbb{R}^d$, $d \in \{1, 2\}$, and let $T > 0$ be the simulation time. Let g denote the gravitational acceleration and let $b : \Omega \longrightarrow \mathbb{R}$ denote a *smooth* function representing the ground elevation measured from a reference altitude (the spatial derivatives of b are often referred to as the bed slope). Let $(x_1, \ldots, x_d)$ denote the spatial coordinates; summation convention for repeated indices is used in the sequel. The SWE can be expressed as follows:

$$\frac{\partial W}{\partial t} + \frac{\partial \mathbb{F}_i(W)}{\partial x_i} = \mathbb{S}(W, b) \quad \text{in } \Omega \times]0, T[\tag{1}$$

Initial and boundary conditions

DOI: 10.1002/fld

where $W:=(h,q):\Omega\times[0,T]\longrightarrow\mathbb{R}^m$, $m:=d+1$, denotes the conservative variables, h being the (scalar-valued) water height (i.e. the thickness of the water flow) and q the ($\mathbb{R}^d$-valued) discharge of the flow with components (q_1,q_2) in two space dimensions. Moreover, the *source term* $\mathbb{S}(W,b)$ and the *flux functions* $\{\mathbb{F}_i(W)\}_{1\leqslant i\leqslant d}$ are defined for $d=1$ as

$$\mathbb{S}(W,b):=\begin{pmatrix}0\\ -gh\dfrac{\partial b}{\partial x_1}\end{pmatrix},\quad \mathbb{F}_1(W):=\begin{pmatrix}q\\ \dfrac{q^2}{h}+\dfrac{g}{2}h^2\end{pmatrix} \tag{2}$$

and for $d=2$ as

$$\mathbb{S}(W,b):=\begin{pmatrix}0\\ -gh\dfrac{\partial b}{\partial x_1}\\ -gh\dfrac{\partial b}{\partial x_2}\end{pmatrix},\quad \mathbb{F}_1(W):=\begin{pmatrix}q_1\\ \dfrac{q_1^2}{h}+\dfrac{g}{2}h^2\\ \dfrac{q_1q_2}{h}\end{pmatrix},\quad \mathbb{F}_2(W):=\begin{pmatrix}q_2\\ \dfrac{q_1q_2}{h}\\ \dfrac{q_2^2}{h}+\dfrac{g}{2}h^2\end{pmatrix} \tag{3}$$

The SWE are presented here without additional terms corresponding to more complex models, such as diffusion, bed friction, Coriolis force, or wind stress source terms. All these additional terms can be discretized using a DG approach. The well-balanced treatment of ground variation effects presented in this paper has to be adapted to other source terms, whenever a steady-state solution at rest still exists. This is the case in the presence of diffusion, Coriolis force, and bed friction since these terms all vanish for a flow at rest. The situation is different in the presence of wind stress effects.

2.2. Space discretization and boundary conditions

Let $\mathscr{T}_\mathscr{D}$ be a shape-regular mesh composed of triangular elements if $d=2$ and of intervals if $d=1$. For simplicity, it is assumed that $\mathscr{T}_\mathscr{D}$ covers Ω exactly, i.e. Ω is a polygonal domain in two space dimensions. Let $\mathfrak{h}:=\max_{K\in\mathscr{T}_\mathscr{D}}\mathfrak{h}_K$, where $\mathfrak{h}_K$ is the diameter of the element $K\in\mathscr{T}_\mathscr{D}$ and let $n_K=(n_{K,1},\ldots,n_{K,d})^t$ be the unit outward normal of K. In one space dimension, n_K is ±1 depending on the orientation. For $K\in\mathscr{T}_\mathscr{D}$, a set $\sigma\subset\partial K$ is said to be an interface (resp., a boundary face) of K if there is $K'\in\mathscr{T}_\mathscr{D}$ with $K'\neq K$ such that $\sigma=K\cap K'$ (resp., if $\sigma=K\cap\partial\Omega$); $E^i_\mathscr{D}(K)$ (resp., $E^\partial_\mathscr{D}(K)$) is then defined as the set of interfaces (resp., boundary faces) of K. In one space dimension, faces are simply nodes. In two space dimensions, if $\mathscr{T}_\mathscr{D}$ does not possess hanging nodes, $E^i_\mathscr{D}(K)$ is simply the set of interior faces of K. Set $E_\mathscr{D}(K)=E^i_\mathscr{D}(K)\cup E^\partial_\mathscr{D}(K)$. For $\sigma\in E^i_\mathscr{D}(K)$, $K\in\mathscr{T}_\mathscr{D}$, K_σ denotes the element of $\mathscr{T}_\mathscr{D}$ sharing the interface σ with K, and for $\sigma\in E_\mathscr{D}(K)$, $n_{K,\sigma}$ denotes the unit outward normal of K on σ and $|\sigma|$ the $(d-1)$-dimensional measure of σ (equal to 1 in one space dimension). The space $\mathbb{P}^p(K)$, $p\in\mathbb{N}$, $K\in\mathscr{T}_\mathscr{D}$, denotes the space of polynomial functions of d variables over K of total degree p at most. The DG space is then defined as $\mathbb{P}^p_\mathscr{D}:=\{v:\Omega\to\mathbb{R}:v|_K\in\mathbb{P}^p(K),\forall K\in\mathscr{T}_\mathscr{D}\}$. Note that a matching condition at interfaces is not enforced on functions in $\mathbb{P}^p_\mathscr{D}$.

For all $K\in\mathscr{T}_\mathscr{D}$, multiply (1) with $v_\mathscr{D}\in[\mathbb{P}^p(K)]^m$, integrate over K, and apply Green's formula (if $d=1$, boundary integrals reduce to a pointwise evaluation). This yields the following

DOI: 10.1002/fld

(continuous-in-time) space approximation of (1): Find $W_{\mathscr{D}} := (h_{\mathscr{D}}, q_{\mathscr{D}}) \in C^1([0,T],[\mathbb{P}^p_{\mathscr{D}}]^m)$ such that $\forall t \in]0,T[$, $\forall K \in \mathscr{T}_{\mathscr{D}}$, $\forall v_{\mathscr{D}} \in [\mathbb{P}^p(K)]^m$:

$$\int_K v_{\mathscr{D}} \frac{\partial W_{\mathscr{D}}}{\partial t} + \int_{\partial K} v_{\mathscr{D}} \phi_K(W_{\mathscr{D}}) - \int_K \frac{\partial v_{\mathscr{D}}}{\partial x_i} \mathbb{F}_i(W_{\mathscr{D}}) = \int_K v_{\mathscr{D}} \mathbb{S}(W_{\mathscr{D}}, b) \tag{4}$$

Initial condition

where $\phi_K(W_{\mathscr{D}})$ is the so-called *numerical flux*. The numerical flux is evaluated as follows: $\forall K \in \mathscr{T}_{\mathscr{D}}$, $\forall \sigma \in E_{\mathscr{D}}(K)$, $\forall x \in \sigma$:

$$\phi_K(W_{\mathscr{D}})(x) = \begin{cases} \phi_*(W_{\mathscr{D}}|_K(x), W_{\mathscr{D}}|_{K_\sigma}(x), n_{K,\sigma}) & \text{if } \sigma \in E^i_{\mathscr{D}}(K) \\ \phi_*(W_{\mathscr{D}}|_K(x), W^\partial_{\mathscr{D}}(x), n_{K,\sigma}) & \text{if } \sigma \in E^\partial_{\mathscr{D}}(K) \end{cases} \tag{5}$$

where $\phi_* : \mathbb{R}^m \times \mathbb{R}^m \times \mathbb{R}^d \longrightarrow \mathbb{R}^m$ is a numerical flux function independent of the mesh cell under consideration and where $W^\partial_{\mathscr{D}}(x)$ is a fictitious outer state that serves to enforce boundary conditions weakly through the numerical fluxes (see below). The functional ϕ_* has to verify certain conditions such as *conservativity*, i.e.

$$\forall (X,Y,n) \in \mathbb{R}^m \times \mathbb{R}^m \times \mathbb{R}^d, \quad \phi_*(X,Y,n) + \phi_*(Y,X,-n) = 0 \tag{6}$$

and *consistency*, i.e.

$$\forall (X,n) \in \mathbb{R}^m \times \mathbb{R}^d, \quad \phi_*(X,X,n) = \mathbb{F}_i(X) n_i \tag{7}$$

In this work, ϕ_* is evaluated using the HLLE flux in one space dimension and the HLLC flux in two space dimensions. The main features of these fluxes are briefly described in Appendix A.

The actual expression for $W^\partial_{\mathscr{D}}(x)$ depends on $W_{\mathscr{D}}|_K(x)$ and on the flow regime where the boundary conditions are enforced. For example, in the case of an inflow boundary face in one space dimension, the speeds of the two Riemann invariants computed using $W_{\mathscr{D}}|_K$ are

$$\lambda_\pm := \frac{q_{\mathscr{D}}|_K}{h_{\mathscr{D}}|_K} \pm \sqrt{g h_{\mathscr{D}}|_K} \tag{8}$$

Observe that $\lambda_+ > 0$ at an inflow boundary. If λ_- is also positive, the flow is said to be *supercritical* and one sets $W^\partial_{\mathscr{D}} = (h^\partial, q^\partial)$, where h^∂ and q^∂ are prescribed values. If λ_- is negative, the flow is said to be *subcritical* and one usually imposes either h or q. More precisely, the conservation of the outward Riemann invariant is expressed in the form

$$\frac{q_{\mathscr{D}}|_K}{h_{\mathscr{D}}|_K} - 2\sqrt{g h_{\mathscr{D}}|_K} = \frac{q^\partial}{h^\partial} - 2\sqrt{g h^\partial} \tag{9}$$

If the outer discharge q^∂ is prescribed, then (9) permits one to obtain an outer water height h^∂ using Newton iterations; if the outer water height h^∂ is prescribed, then (9) immediately yields an outer discharge q^∂. In two space dimensions, there are three Riemann invariants; two speeds are evaluated as in (8) using the normal discharge $n_{K,\sigma} \cdot q_{\mathscr{D}}|_K$ while the last speed is given by the ratio $n_{K,\sigma} \cdot q_{\mathscr{D}}|_K / h_{\mathscr{D}}|_K$. The above procedure is modified accordingly in a straightforward manner. For a thorough discussion of boundary conditions for SWE and fictitious outer states, we refer to [5, 37].

DOI: 10.1002/fld

To express (4) in vector form, a set of basis functions in $[\mathbb{P}^p_{\mathscr{D}}]^m$ must be selected. To exploit the local character of DG methods, the basis functions have support localized at a single mesh cell. On a given mesh cell, the local basis functions are Legendre polynomials in one space dimension and a particular set of modal basis functions constructed using barycentric coordinates in two space dimensions (see [38] for some properties of these modal basis functions). Let $\mathbf{W}_{\mathscr{D}} \in \mathbb{R}^N$ denote the component vector of $W_{\mathscr{D}}$ with respect to the basis functions; here, N denotes the total number of degrees of freedom, i.e. the dimension of $[\mathbb{P}^p_{\mathscr{D}}]^m$ ($N = Mm((p+d)!/d!p!)$, where M denotes the number of mesh cells). Then, upon inverting the mass matrix, (4) can be recast into the form

$$\frac{\mathrm{d}\mathbf{W}_{\mathscr{D}}}{\mathrm{d}t} = \mathscr{H}_{\mathscr{D}}(\mathbf{W}_{\mathscr{D}}) \tag{10}$$

where $\mathscr{H}_{\mathscr{D}} : \mathbb{R}^N \to \mathbb{R}^N$. Observe that the mass matrix is block diagonal and hence easily invertible.

2.3. Time discretization

The discretization of (10) is performed in a fully explicit way. This explicit time discretization can become a concern in complex applications, in particular whenever some elements in the unstructured triangular mesh are very small or badly shaped, leading to a severe stability condition on the time step Δt in both cases. This problem can be handled by correcting the mesh (which is not always an actual solution) or by using local time stepping [38, 39].

Let $(t^k)_{k\in\mathbb{N}}$ be a sequence of discrete times with $t^0 = 0$. Let $(\Delta t)^k = t^{k+1} - t^k$ be the $(k+1)$th time step. To construct an approximation $\mathbf{W}^k_{\mathscr{D}}$ of $\mathbf{W}_{\mathscr{D}}$ at the discrete time t^k, a Runge–Kutta (RK) scheme of order q is used. Given an initial condition $\mathbf{W}^0_{\mathscr{D}}$, the scheme consists of the following steps: For $k \in \mathbb{N}$, set $\mathbf{W}^{k+1,0}_{\mathscr{D}} = \mathbf{W}^k_{\mathscr{D}}$, then for $i \in \{1, \ldots, q\}$, compute the RK sub-iterates

$$\mathbf{W}^{k+1,i}_{\mathscr{D}} = \sum_{l=0}^{i-1} c_i^l \mathbf{w}^l_{\mathscr{D},i}, \quad \mathbf{w}^l_{\mathscr{D},i} = \mathbf{W}^{k+1,l}_{\mathscr{D}} + \frac{d_i^l}{c_i^l}(\Delta t)^k \mathscr{H}_{\mathscr{D}}(\mathbf{W}^{k+1,l}_{\mathscr{D}}) \tag{11}$$

and finally set $\mathbf{W}^{k+1}_{\mathscr{D}} = \mathbf{W}^{k+1,q}_{\mathscr{D}}$. The coefficients c_i^l and d_i^l in (11) can be found in [16]. To ensure an equal order of accuracy in space and time, an RK scheme of order $(p+1)$ is used, i.e. $q = p+1$.

The time step is determined adaptively by taking $(\Delta t)^k := \min((\Delta t)^*, \alpha(\Delta t)^k_{\mathrm{cfl}})$, where $(\Delta t)^*$ is a user-defined maximal time step, $\alpha = 0.5$ and $(\Delta t)^k_{\mathrm{cfl}}$ results from the following Courant–Friedrichs–Lewy condition [16]:

$$(\Delta t)^k_{\mathrm{cfl}} := \frac{1}{2p+1} \min_{K\in\mathscr{T}_{\mathscr{D}}} \left[\frac{\mathfrak{h}_K}{\sup_{\partial K} \left(\left| \frac{q^k_{\mathscr{D}}}{h^k_{\mathscr{D}}} \cdot n_K \right| + \sqrt{g h^k_{\mathscr{D}}} \right)} \right] \tag{12}$$

Here, $W^k_{\mathscr{D}} = (h^k_{\mathscr{D}}, q^k_{\mathscr{D}})$ is the function in $[\mathbb{P}^p_{\mathscr{D}}]^m$ associated with the component vector $\mathbf{W}^k_{\mathscr{D}}$.

2.4. Slope limiting

It is well known that in the context of conservation laws, a shock can appear in finite time even if the initial data are smooth. Moreover, high-order methods can yield spurious oscillations near a

DOI: 10.1002/fld

shock. To avoid this situation, slope limiting is necessary. Slope limiting consists of replacing the evaluation of $\mathbf{W}_{\mathscr{D}}^{k+1,i}$ in (11) by

$$\mathbf{W}_{\mathscr{D}}^{k+1,i}=\Lambda_i\left(\sum_{l=0}^{i-1}c_i^l\mathbf{w}_{\mathscr{D},i}^l\right),\quad \mathbf{w}_{\mathscr{D},i}^l=\mathbf{W}_{\mathscr{D}}^{k+1,l}+\frac{d_i^l}{c_i^l}(\Delta t)^k\mathscr{H}_{\mathscr{D}}(\mathbf{W}_{\mathscr{D}}^{k+1,l}) \tag{13}$$

noting that the evaluation of $\mathbf{w}_{\mathscr{D},i}^l$ is kept unchanged [16]. Here, $\Lambda_i:\mathbb{R}^N\to\mathbb{R}^N$, $i\in\{1,\ldots,q\}$, are operators that firstly detect shocks and mark cells near shocks and then, on the marked cells, restrict the polynomial order to $p=1$ and reconstruct the slope of the approximation using mean-preserving transformations. In [16], the same operator $\Lambda_i\equiv\Lambda$ is used at each RK sub-iterate. Here, this technique is used in one space dimension, but to reduce computational costs in two space dimensions, Λ_i is the identity for $i<q$ and $\Lambda_q\equiv\Lambda$, that is, slope limiting is enforced only on the last RK sub-iterate. Furthermore, following the ideas of [18], slope limiting is applied to the free surface elevation $(h+b)$ rather than to the water height h. The motivation for this choice is that if the bed slope is nonzero, the limitation procedure should lead to a constant flow elevation instead of a constant flow height when the flow is close to a steady state at rest. To detect shocks, the criterion proposed in [40] is used. For all $K\in\mathscr{T}_{\mathscr{D}}$, define the subset $E_{\mathscr{D}}^-(K)$ of $E_{\mathscr{D}}(K)$ as the inflow interfaces or boundary faces of K, namely

$$E_{\mathscr{D}}^-(K):=\left\{\sigma\in E_{\mathscr{D}}(K):\int_\sigma q_{\mathscr{D}}\cdot n_{K,\sigma}\leqslant 0\right\} \tag{14}$$

Then, setting for all $K\in\mathscr{T}_{\mathscr{D}}$ and for all $\sigma\in E_{\mathscr{D}}(K)$,

$$\mathscr{I}_{K,\sigma}:=\frac{|\int_\sigma(h_{\mathscr{D}}|_K-h_{\mathscr{D}}|_{K_\sigma})|}{\mathfrak{h}_K^{(p+1)/2}|\sigma||\langle h_{\mathscr{D}}\rangle_K|},\quad \mathscr{I}_K:=\sum_{\sigma\in E_{\mathscr{D}}^-(K)}\mathscr{I}_{K,\sigma} \tag{15}$$

where $\langle h_{\mathscr{D}}\rangle_K$ denotes the mean value of $h_{\mathscr{D}}$ over K, the criterion is to apply slope limiting on K whenever $\mathscr{I}_K\geqslant 1$. The motivation for using the above detection criterion stems from the observation that smooth DG solutions often exhibit a superconvergence behavior at outflow boundaries of mesh cells; we refer to [40] and references therein for more details.

3. A WELL-BALANCED RKDG SCHEME WITH FLUX MODIFICATION

The preservation of equilibrium states is a desirable feature for schemes dealing with the SWE. Among these states, we will consider in particular *steady states at rest*. These states are defined by the conditions $h+b\equiv C$ (a constant) and $q\equiv 0$ over the domain. Failure to preserve such states leads to so-called *numerical waves*; see, e.g. [41] for an example with FV methods and Section 5.2.1 for an example with DG methods. Approximation schemes that avoid this situation are termed *well-balanced schemes*. In the context of the SWE, another terminology is the 'exact C-property' introduced in [9]; it means that the scheme preserves the states such that $h+b\equiv C$ and $q\equiv 0$. The RKDG scheme defined in Section 2 is not well balanced, i.e. does not satisfy the exact C-property. The goal of this section is to cure this difficulty. A well-balanced DG scheme for the SWE has already been proposed in [30]. The present scheme is somewhat different; a comparison is given at the end of this section.

DOI: 10.1002/fld

A first observation is that it is not possible to obtain $h_{\mathscr{D}}+b\equiv C$ simply because $b\notin\mathbb{P}^p_{\mathscr{D}}$. Hence, we seek for the optimal $h_{\mathscr{D}}\in\mathbb{P}^p_{\mathscr{D}}$ in the least-squares sense, that is, we seek for $h_{\mathscr{D}}\in\mathbb{P}^p_{\mathscr{D}}$ such that $h_{\mathscr{D}}+b_{\mathscr{D}}\equiv C$, where $b_{\mathscr{D}}\in\mathbb{P}^p_{\mathscr{D}}$ is the L^2-projection of b onto $\mathbb{P}^p_{\mathscr{D}}$. Recall that this projection verifies

$$\int_K bv_{\mathscr{D}}=\int_K b_{\mathscr{D}}v_{\mathscr{D}}\quad\forall v_{\mathscr{D}}\in\mathbb{P}^p(K)\quad\forall K\in\mathscr{T}_{\mathscr{D}} \tag{16}$$

The well-balanced RKDG scheme with slope limiting is obtained by modifying (4) as follows:

$$\begin{aligned}\int_K v_{\mathscr{D}}\frac{\partial W_{\mathscr{D}}}{\partial t}+\int_{\partial K}v_{\mathscr{D}}\phi_K(W^{\diamond}_{\mathscr{D}})-\int_K\frac{\partial v_{\mathscr{D}}}{\partial x_i}\mathbb{F}_i(W_{\mathscr{D}})\\ =\int_K v_{\mathscr{D}}\mathbb{S}(W_{\mathscr{D}},b_{\mathscr{D}})+\int_{\partial K}v_{\mathscr{D}}\delta_K(W_{\mathscr{D}},b_{\mathscr{D}})\end{aligned} \tag{17}$$

Here, $W^{\diamond}_{\mathscr{D}}$ is a modified state, obtained according to the hydrostatic reconstruction of the water height proposed in [29]. It is given by $W^{\diamond}_{\mathscr{D}}:=(h^{\diamond}_{\mathscr{D}},q^{\diamond}_{\mathscr{D}})$ with $q^{\diamond}_{\mathscr{D}}:=h^{\diamond}_{\mathscr{D}}q_{\mathscr{D}}/h_{\mathscr{D}}$ and for $K\in\mathscr{T}_{\mathscr{D}}$,

$$h^{\diamond}_{\mathscr{D}}|_K:=\begin{cases}\max(0,h_{\mathscr{D}}|_K-\max(b_{\mathscr{D}}|_{K_\sigma}-b_{\mathscr{D}}|_K,0)), & \sigma\in E^i_{\mathscr{D}}(K)\\ h_{\mathscr{D}}|_K, & \sigma\in E^{\partial}_{\mathscr{D}}(K)\end{cases} \tag{18}$$

Furthermore,

$$\delta_K(W_{\mathscr{D}},b_{\mathscr{D}}):=\begin{pmatrix}0\\ \dfrac{g}{2}(h^{\diamond}_{\mathscr{D}}|^2_K-h_{\mathscr{D}}|^2_K)n_K\end{pmatrix} \tag{19}$$

The difference between (4) and (17) is on the one hand that in (17), the numerical flux is evaluated using $W^{\diamond}_{\mathscr{D}}$ instead of $W_{\mathscr{D}}$ (still using (5)), and on the other hand that the source term consists of a volume contribution $\int_K v_{\mathscr{D}}\mathbb{S}(W_{\mathscr{D}},b_{\mathscr{D}})$ (evaluated using the projected ground elevation $b_{\mathscr{D}}$) and a surface contribution $\int_{\partial K}v_{\mathscr{D}}\delta_K(W_{\mathscr{D}},b_{\mathscr{D}})$. In vector form, (17) can be recast into the form

$$\frac{\mathrm{d}\mathbf{W}_{\mathscr{D}}}{\mathrm{d}t}=\mathscr{H}^{\mathrm{wb}}_{\mathscr{D}}(\mathbf{W}_{\mathscr{D}})$$

where $\mathscr{H}^{\mathrm{wb}}_{\mathscr{D}}:\mathbb{R}^N\to\mathbb{R}^N$. The well-balanced RKDG scheme consists of replacing (13) by

$$\mathbf{W}^{k+1,i}_{\mathscr{D}}=\Lambda_i\left(\sum_{l=0}^{i-1}c^l_i\mathbf{w}^l_{\mathscr{D},i}\right),\quad\mathbf{w}^l_{\mathscr{D},i}=\mathbf{W}^{k+1,l}_{\mathscr{D}}+\frac{d^l_i}{c^l_i}(\Delta t)^k\mathscr{H}^{\mathrm{wb}}_{\mathscr{D}}(\mathbf{W}^{k+1,l}_{\mathscr{D}}) \tag{20}$$

The key property of the above scheme is given as follows.

Proposition 1
The scheme (20) preserves steady states at rest, i.e. for all $k\in\mathbb{N}$:

$$(h^k_{\mathscr{D}}+b_{\mathscr{D}}\equiv C\text{ and }q^k_{\mathscr{D}}\equiv 0)\Rightarrow(h^{k+1}_{\mathscr{D}}+b_{\mathscr{D}}\equiv C\text{ and }q^{k+1}_{\mathscr{D}}\equiv 0) \tag{21}$$

where C denotes a fixed positive constant.

DOI: 10.1002/fld

Proof
Let $W_{\mathscr{D}}=(h_{\mathscr{D}},q_{\mathscr{D}})\in[\mathbb{P}^p_{\mathscr{D}}]^m$ such that $h_{\mathscr{D}}+b_{\mathscr{D}}\equiv C$ and $q_{\mathscr{D}}=0$ (the superscript k is omitted for brevity). We set $d=2$ for this proof, the case $d=1$ is treated in a similar way. It is clear that it is sufficient to prove that for all $K\in\mathscr{T}_{\mathscr{D}}$ and for all $v_{\mathscr{D}}\in[\mathbb{P}^p(K)]^m$,

$$\int_{\partial K} v_{\mathscr{D}}\phi_K(W^{\diamond}_{\mathscr{D}})-\int_K \frac{\partial v_{\mathscr{D}}}{\partial x_i}\mathbb{F}_i(W_{\mathscr{D}})=\int_K v_{\mathscr{D}}\mathbb{S}(W_{\mathscr{D}},b_{\mathscr{D}})+\int_{\partial K} v_{\mathscr{D}}\delta_K(W_{\mathscr{D}},b_{\mathscr{D}})$$

Since $W_{\mathscr{D}}$ corresponds to a steady state at rest, it is readily verified that

- for all $K\in\mathscr{T}_{\mathscr{D}}$ and for all $\sigma\in E^i_{\mathscr{D}}(K)$, $h^{\diamond}_{\mathscr{D}}$ is single valued on σ and equal to $C-\max(b_{\mathscr{D}}|_K,b_{\mathscr{D}}|_{K_\sigma})$;
- $q^{\diamond}_{\mathscr{D}}=0$.

Using the consistency of the flux function ϕ_* (see (7)) then yields

$$\phi_K(W^{\diamond}_{\mathscr{D}})=\begin{pmatrix}0\\ \dfrac{g}{2}(h^{\diamond}_{\mathscr{D}}|_K)^2 n_{K,1}\\ \dfrac{g}{2}(h^{\diamond}_{\mathscr{D}}|_K)^2 n_{K,2}\end{pmatrix}$$

Moreover,

$$\mathbb{F}_1(W):=\begin{pmatrix}0\\ \dfrac{g}{2}h^2_{\mathscr{D}}\\ 0\end{pmatrix},\quad \mathbb{F}_2(W):=\begin{pmatrix}0\\ 0\\ \dfrac{g}{2}h^2_{\mathscr{D}}\end{pmatrix},\quad \mathbb{S}(W_{\mathscr{D}},b_{\mathscr{D}}):=\begin{pmatrix}0\\ \dfrac{g}{2}\dfrac{\partial h^2_{\mathscr{D}}}{\partial x_1}\\ \dfrac{g}{2}\dfrac{\partial h^2_{\mathscr{D}}}{\partial x_2}\end{pmatrix}$$

where we have used that $h_{\mathscr{D}}+b_{\mathscr{D}}\equiv C$ in the expression for $\mathbb{S}(W_{\mathscr{D}},b_{\mathscr{D}})$. Using (19) and Green's formula yields the desired result. □

Remark 1
The only property required on the numerical flux for the above result to hold is consistency (but not conservativity).

It is important to assess the accuracy of the above flux modification technique. This motivates the following.

Proposition 2
Let $W_{\mathscr{D}}\in[\mathbb{P}^p_{\mathscr{D}}]^m$. Assume that for all $K\in\mathscr{T}_{\mathscr{D}}$, $h_{\mathscr{D}}|_K$ is positive and that $h_{\mathscr{D}}|_K$ and $(q_{\mathscr{D}}/h_{\mathscr{D}})|_K$ are uniformly bounded. Assume that the ground elevation is smooth enough. Then, for all $K\in\mathscr{T}_{\mathscr{D}}$, for all $\sigma\in E^i_{\mathscr{D}}(K)$, and for all $x\in\sigma$,

$$\|W_{\mathscr{D}}(x)-W^{\diamond}_{\mathscr{D}}(x)\|_{\mathbb{R}^m}+\|\delta_K(W_{\mathscr{D}},b_{\mathscr{D}})\|_{\mathbb{R}^m}\leqslant c\mathfrak{h}_K^{p+1} \tag{22}$$

where c is independent of $\mathscr{T}_{\mathscr{D}}$ and where $\|\cdot\|_{\mathbb{R}^m}$ denotes any norm on $\mathbb{R}^m$.

DOI: 10.1002/fld

Proof
Since the ground elevation is smooth enough, classical approximation results imply that for all $K \in \mathcal{T}_{\mathscr{D}}$, for all $\sigma \in E^i_{\mathscr{D}}(K)$, and for all $x \in \sigma$,

$$|b_{\mathscr{D}}|_K(x) - b_{\mathscr{D}}|_{K_\sigma}(x)| \leqslant c\mathfrak{h}_K^{p+1}$$

from where the conclusion is readily inferred. □

Proposition 2 shows that the flux modification technique induces a perturbation of the original RKDG scheme of order h^{p+1}. Since the problem is nonlinear, it cannot be inferred that the error induced by this perturbation is necessarily of the same order. Numerical results reported in Section 5 confirm that the present flux modification technique preserves the high-order accuracy of the RKDG method.

Although both schemes involve a modification of the flux and of the source term, the present well-balanced DG scheme and that proposed in [30] exhibit some differences. In the former, the same numerical fluxes are used, but they are evaluated at the modified state $W^{\diamond}_{\mathscr{D}}$ which is designed to be single valued at interfaces whenever the discrete solution corresponds to a steady flow at rest; in the latter, the centered part of the numerical flux is evaluated at the original state $W_{\mathscr{D}}$, while the noncentered part of the flux is evaluated using some invariants associated with the steady flow at rest (these invariants are single valued at interfaces whenever the discrete solution corresponds to a steady flow at rest). Concerning the evaluation of the source term, both schemes introduce additional terms (involving the L^2-projection of b onto $\mathbb{P}^p_{\mathscr{D}}$); the present well-balanced DG scheme introduces only a high-order boundary perturbation, whereas the scheme proposed in [30] first splits the source term into two contributions using the invariants associated with the steady flow at rest and then integrates by parts one of the contributions, yielding high-order boundary perturbations.

4. SLOPE MODIFICATION FOR FLOODING AND DRYING

When the problem involves flooding and drying, it is necessary to prevent the discrete water height from taking negative values. To this purpose, an additional slope modification is applied on each mesh cell where the minimum (computed over the integration points) of $h_{\mathscr{D}}$ is lower than a threshold ε. The procedure is performed separately on each single mesh element. It is similar in spirit to that used in the context of reentry hypersonic flows in compressible gas dynamics where the computed air density has to remain positive whenever near-vacuum regions appear in the domain during the computation [42]. For the SWE, a more sophisticated procedure has been derived in [32]; the extension of this procedure to DG methods will not be explored here.

Let $K \in \mathcal{T}_{\mathscr{D}}$. For $p=0$, the procedure is similar to the standard procedure used in FV, namely setting $h_{\mathscr{D}}$ and $q_{\mathscr{D}}$ to zero. For $p \geqslant 2$, the discrete solution is first projected onto linears and then the procedure for $p=1$ is applied elementwise as follows:

- If the average of $h_{\mathscr{D}}$ is negative, then $h_{\mathscr{D}}$ and $q_{\mathscr{D}}$ are set to zero.
- If the average of $h_{\mathscr{D}}$ is nonnegative, this value is kept but the gradient of $h_{\mathscr{D}}$ is modified in such a way that $h_{\mathscr{D}}$ vanishes at vertices with negative value. Since $h_{\mathscr{D}}|_K$ is affine, it is sufficient to modify its value at the vertices of the given mesh cell K. Moreover, since we are working with discontinuous approximations, this procedure can be applied elementwise. More specifically in two space dimensions, let K be the reference triangle with vertices $v_0 := (0,0)$,

DOI: 10.1002/fld

$v_1 := (1,0)$, and $v_2 := (0,1)$. Introduce the nodal polynomial basis functions $p_0 := 1-x-y$, $p_1 := x$, and $p_2 := y$. Let $h_{\mathscr{D}} \in \mathbb{P}^1(K)$ be such that $h_{\mathscr{D}} := \sum_{j=0}^{2} h_j p_j$ and assume that $h_{\mathscr{D}}$ has negative values on K. Let $\langle h_{\mathscr{D}} \rangle_K$ denote the mean of $h_{\mathscr{D}}$ over K. If $h_{\mathscr{D}}$ is negative at only one vertex, say v_i with $i \in \{0,1,2\}$, then the new water height $h'_{\mathscr{D}}$ is

$$h'_{\mathscr{D}} := \frac{\langle h_{\mathscr{D}} \rangle_K}{\langle h_{\mathscr{D}} \rangle_K - h_i} (h_{\mathscr{D}} - h_i) \tag{23}$$

If $h_{\mathscr{D}}$ is negative at two vertices, say v_{i_1} and v_{i_2} with $i_1, i_2 \in \{0,1,2\}$, then the new water height $h'_{\mathscr{D}}$ is

$$h'_{\mathscr{D}} := \frac{\langle h_{\mathscr{D}} \rangle_K}{\langle p_i \rangle_K} p_i \tag{24}$$

where $i \in \{0,1,2\} \setminus \{i_1, i_2\}$. It is straightforward to verify that in both cases,

$$\langle h'_{\mathscr{D}} \rangle_K = \langle h_{\mathscr{D}} \rangle_K \tag{25}$$

$$\forall x \in K, \quad h'_{\mathscr{D}}(x) \geqslant 0 \tag{26}$$

Finally, the discharge $q_{\mathscr{D}}$ is modified by only setting its value to zero at those vertices where $h_{\mathscr{D}}$ has been modified. Hence, any modification of the water height at a vertex is accompanied by setting the discharge $q_{\mathscr{D}}$ to zero at that vertex. Moreover, to avoid large spurious values of the discrete velocity norm (larger than a prescribed upper bound for the velocity in the flow) in those mesh cells where the water height $h_{\mathscr{D}}$ has been limited as described above, an additional limiting is applied to the discharge $q_{\mathscr{D}}$ at each vertex where the water height $h_{\mathscr{D}}$ is small but positive and the discharge $q_{\mathscr{D}}$ is not small. The limiting of the discharge is applied only if the water depth is (very) small. The overall transformation of $(h_{\mathscr{D}}, q_{\mathscr{D}})$ preserves mass because of (25) (as long as the average of $h_{\mathscr{D}}$ is nonnegative) but not the mean value of the discharge.

Let $\Upsilon : \mathbb{R}^N \to \mathbb{R}^N$ denote the mean-preserving and nonnegativity-enforcing transformation defined above, transforming the state $W_{\mathscr{D}} = (h_{\mathscr{D}}, q_{\mathscr{D}})$ into $\Upsilon(W_{\mathscr{D}}) = (h'_{\mathscr{D}}, q'_{\mathscr{D}})$, where $h'_{\mathscr{D}}$ is obtained *via* (23)–(26) and $q'_{\mathscr{D}}$ is limited as described above. The well-balanced RKDG scheme with slope modification consists of replacing (20) by

$$\mathbf{W}_{\mathscr{D}}^{k+1,i} = \Lambda_i \left(\sum_{l=0}^{i-1} c_i^l \mathbf{w}_{\mathscr{D},i}^l \right), \quad \mathbf{w}_{\mathscr{D},i}^l = \mathbf{W}_{\mathscr{D}}^{k+1,l} + \frac{d_i^l}{c_i^l} (\Delta t)^k \mathscr{H}_{\mathscr{D}}^{\mathrm{wb}} [\Upsilon(\mathbf{W}_{\mathscr{D}}^{k+1,l})] \tag{27}$$

Slope limiting is not applied at the same time as slope modification, since the latter can artificially activate the former.

5. NUMERICAL TESTS

Test cases presented in this section are regrouped into three subsections. In Section 5.1, we illustrate the ability of the classical RKDG scheme described in Section 2 to approximate smooth solutions with high accuracy and to capture sharply shocks for constant ground elevation. In Section 5.2, we illustrate the fact that the well-balanced RKDG scheme designed in Section 3 performs equally

DOI: 10.1002/fld

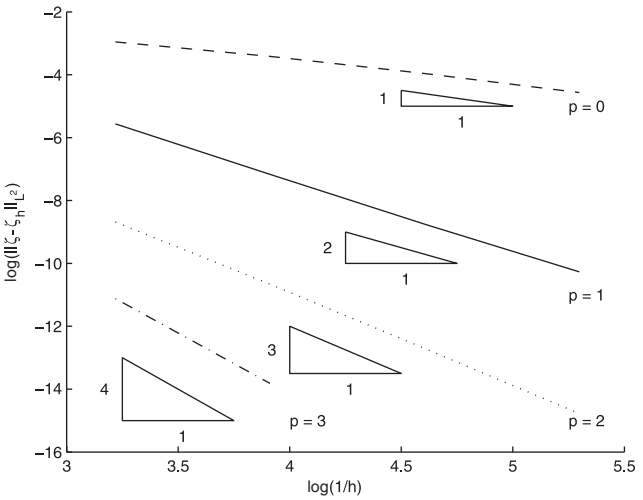

Figure 1. Test case with smooth solution: L^2-error on the water height for $p \in \{0, 1, 2, 3\}$.

well in terms of accuracy and shock capturing when the ground elevation is variable. In Section 5.3, we assess the slope modification technique designed in Section 4 to handle flooding and drying within the well-balanced RKDG scheme. In the sequel, we set $g = 9.81\,\mathrm{m/s^2}$. When evaluating convergence rates below, the parameter $\mathfrak{h}$ representative of a given triangulation is evaluated as the maximal length of an edge in the triangulation. The unstructured meshes considered henceforth are shape regular (in general, the minimal length of an edge in the mesh is larger than $\mathfrak{h}/3$). We consider that a steady-state solution is reached whenever the transient residual (the difference between two successive approximate solutions) goes under a given threshold (in general 10^{-7} times the initial residual). In some cases however (in general those involving shocks), the transient residual did not converge to zero, but oscillated around a given level (owing to an oscillating activation of limiters). In this case, the solution is considered as steady after a sufficiently large number of time iterations. Finally, let us recall that the time step is variable and set according to (12) and that, if a $\mathbb{P}^p$ DG method is used, an RK scheme of order $(p+1)$ is used to ensure an equal order of accuracy in space and time.

5.1. Constant ground elevation

5.1.1. Smooth solutions. Consider a one-dimensional domain Ω of length 10 m and a final simulation time of $T = 0.5\,\mathrm{s}$. The initial datum is a perturbation of the steady state at rest with $h = 1\,\mathrm{m}$. It is given by $h_0 = (1 + 0.2\mathrm{e}^{-100(x-0.5)^2})\,\mathrm{m}$ and $q_0 = 0\,\mathrm{m^2/s}$. Because the simulation time is small enough, the perturbation does not reach the boundaries of the domain. Since an analytical solution is not available, the error is calculated with respect to a reference solution computed on a uniform mesh of 200 cells with polynomial degree $p = 3$. Figure 1 presents the L^2-error on the water height for various mesh sizes. In all cases, the convergence rate is $(p+1)$ as expected.

5.1.2. Oblique hydraulic jump. The aim of this test case is to study the performance of the classical RKDG scheme in the case where the exact solution presents a shock. We consider the standard test

DOI: 10.1002/fld

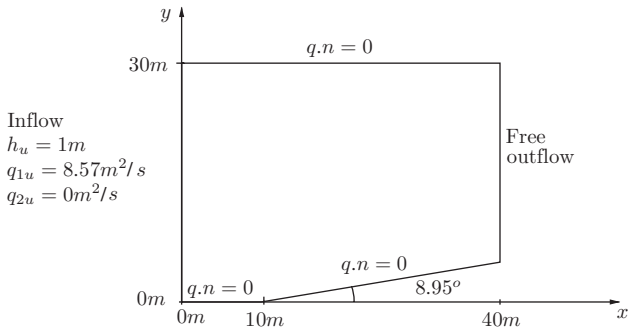

Figure 2. Oblique hydraulic jump: problem setting.

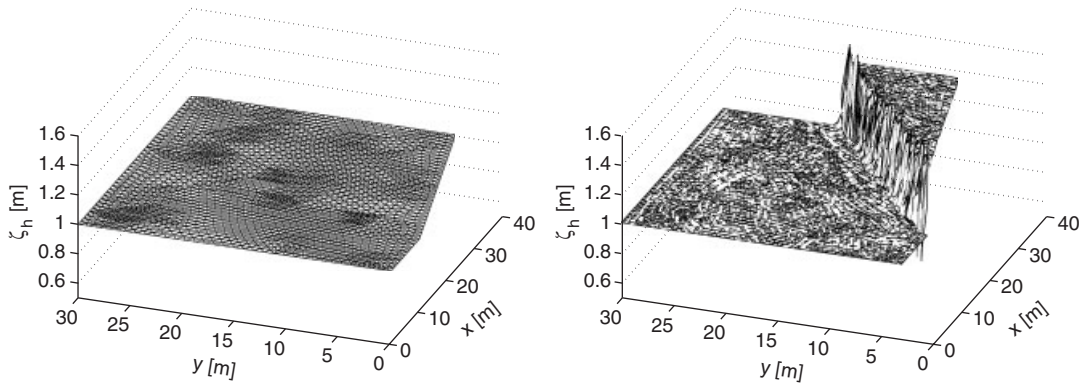

Figure 3. Oblique hydraulic jump: initial (left) and final (right) approximate water heights for $p=1$.

case of an oblique hydraulic jump on a flat bottom [43]. The definition of the problem is illustrated in Figure 2: a uniform horizontal inflow (state (h_u, q_{1u}, q_{2u}) with $q_{2u}=0\,\mathrm{m}^2/\mathrm{s}$) is deflected by an oblique wall with deflection angle α. The steady analytical solution presents an oblique jump (angle β with the horizontal axis) separating the inflow zone from a constant downstream state (h_d, q_{1d}, q_{2d}) with $(q_{1d}, q_{2d}) = q_d(\cos(\alpha), \sin(\alpha))$. The *Rankine–Hugoniot* jump relations yield

$$q_{1u}^2 \sin^2\beta = q_d^2 \sin^2(\beta-\alpha) = g h_u h_d \frac{h_u+h_d}{2}, \quad \tan(\alpha) = \frac{(h_d-h_u)\sin\beta}{h_u \sin^2\beta + h_d \cos^2\beta}$$

Imposing $h_u=1\,\mathrm{m}$, $h_d=1.5\,\mathrm{m}$, and $\beta=30^\circ$ yields the approximate values: $\alpha\approx 8.9483^\circ$, $q_{1u}\approx 8.5776\,\mathrm{m}^2/\mathrm{s}$, $(q_{1d}, q_{2d})\approx(11.7941, 1.8571)\,\mathrm{m}^2/\mathrm{s}$. Furthermore, the initial condition is $h_0=1\,\mathrm{m}$ and $q_0=(8.57, 0)\,\mathrm{m}^2/\mathrm{s}$. We compute the DG solution on unstructured meshes for the degree of approximation $p=1$. For this test case, the steady-state solution is reached after $T=10\,\mathrm{s}$. The typical time step is $\Delta t=0.00168\,\mathrm{s}$ for the finest mesh (for which $h=0.464\,\mathrm{m}$). The initial and final (i.e. steady state) approximations are represented in Figure 3. For all the conserved variables, the convergence rate of the L^2-error is $\frac{1}{2}$ as expected owing to the presence of a shock and the use of unfitted meshes (i.e. the oblique shock crosses some mesh cells).

DOI: 10.1002/fld

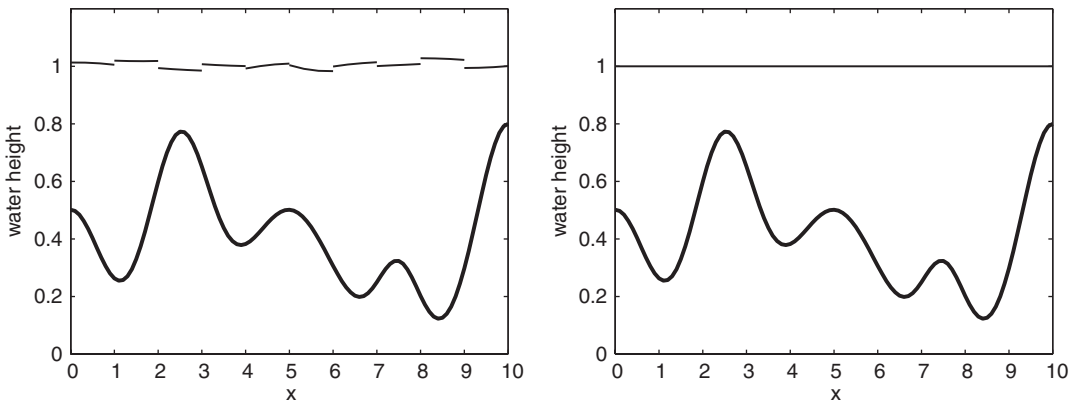

Figure 4. Steady state at rest: ground and free surface elevations for the classical RKDG scheme (left) and for the well-balanced RKDG scheme (right) for $p=2$ at time $T=1\,\mathrm{s}$ (ground elevation in bold line).

5.2. *Variable ground elevation*

5.2.1. Steady state at rest. The preservation of steady states at rest by the well-balanced RKDG scheme is illustrated on a one-dimensional setting. The initial condition is $h_0+b=1\,\mathrm{m}$ and $q_0=(0,0)\,\mathrm{m}^2/\mathrm{s}$ with $b(x)=(10\mathrm{e}^{-x^2}+15\mathrm{e}^{-(x-2.5)^2}+10\mathrm{e}^{-(x-5)^2/2}+6\mathrm{e}^{-2(x-7.5)^2}+16\mathrm{e}^{-(x-10)^2})/20$. Figure 4 presents the approximate solution at time $T=1\,\mathrm{s}$ obtained by the classical RKDG scheme and by the well-balanced RKDG scheme for $p=2$ and a uniform step size of $h=1\,\mathrm{m}$. The importance of numerical waves introduced by the classical scheme and their elimination by the flux modification technique are clearly illustrated.

5.2.2. Subcritical flow. To assess the order of accuracy of the well-balanced RKDG scheme, we consider a classical test case of a subcritical flow over a bump [44]. The definition of the problem is illustrated in Figure 5. The ground elevation is $b(x,y)=\max(0,0.2-0.05(x-10)^2)$ and the initial condition $h_0+b=2\,\mathrm{m}$ and $q_0=(0,0)\,\mathrm{m}^2/\mathrm{s}$. The incoming discharge is $q_1=4.42\,\mathrm{m}^2/\mathrm{s}$, $q_2=0\,\mathrm{m}^2/\mathrm{s}$, and the downwind water height is fixed to $h_{\mathrm{out}}=2\,\mathrm{m}$. After a finite time (between $T=10$ and $60\,\mathrm{s}$), the solution reached a steady state (see Figure 6). For this case, the typical number of iterations is 10 000, and the time step for $p=2$ is $\Delta t=0.00115\,\mathrm{s}$ for the finest unstructured mesh (for which $h=0.234\,\mathrm{m}$). Using structured, fitted meshes in which the lines of discontinuity of the ground slope coincide with mesh cell interfaces, the optimal order of convergence $(p+1)$ of the RKDG method is recovered. The errors in the L^2-norm on the water height for $p\in\{0,1,2\}$ are plotted in the left part of Figure 7. Using unstructured, unfitted meshes, the optimal order of convergence $(p+1)$ of the RKDG method is not preserved. The errors in the L^2-norm on the water height for $p\in\{0,1,2\}$ are plotted in the right part of Figure 7. The maximum order of convergence is $\frac{3}{2}$; this can be explained by the fact that the exact solution is continuous but not continuously differentiable inside some mesh elements.

5.2.3. Transcritical flow with shock. We consider the same domain and ground elevation as in the previous test case but the initial condition is $h_0+b=0.33\,\mathrm{m}$ and $q_0=(0,0)\,\mathrm{m}^2/\mathrm{s}$. Moreover, the inflow discharge and the outflow water height are $q_{\mathrm{in}}=(0.18,0)\,\mathrm{m}^2/\mathrm{s}$ and $h_{\mathrm{out}}=0.33\,\mathrm{m}$ [44].

DOI: 10.1002/fld

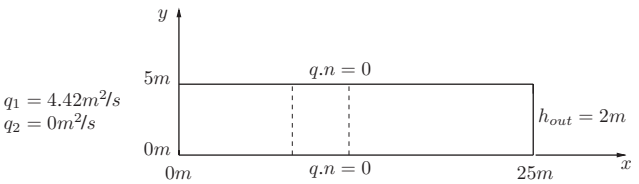

Figure 5. Subcritical flow: problem setting (the leading and trailing edges of the bump are indicated by a dashed line).

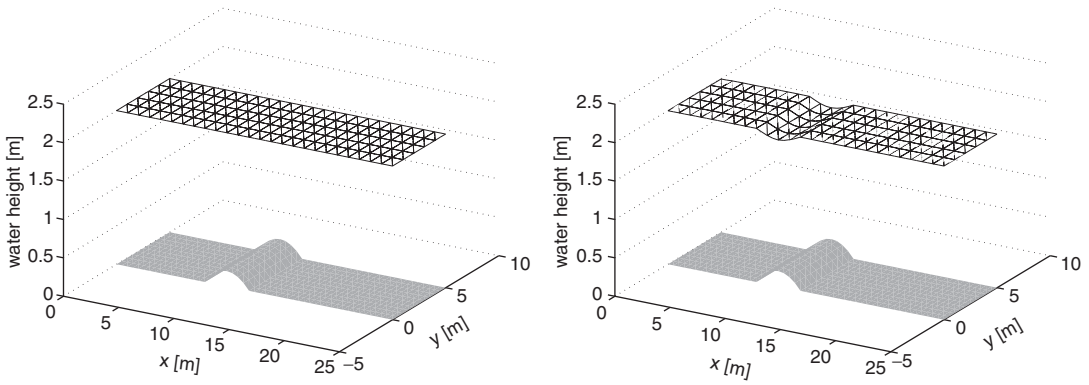

Figure 6. Subcritical flow: initial (left) and final (right) approximate water heights for $p=1$ (structured, fitted meshes).

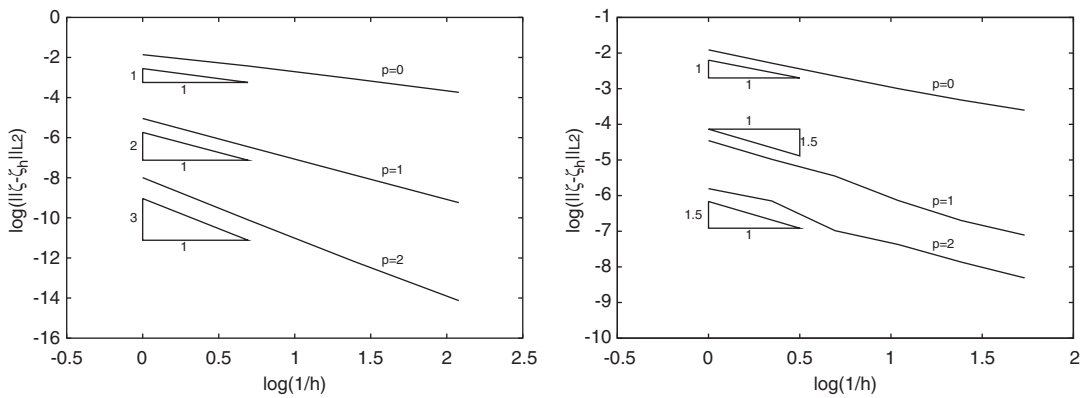

Figure 7. Subcritical flow: L^2-error on the water height for $p \in \{0,1,2\}$: structured, fitted meshes (left) and unstructured, unfitted meshes (right).

DOI: 10.1002/fld

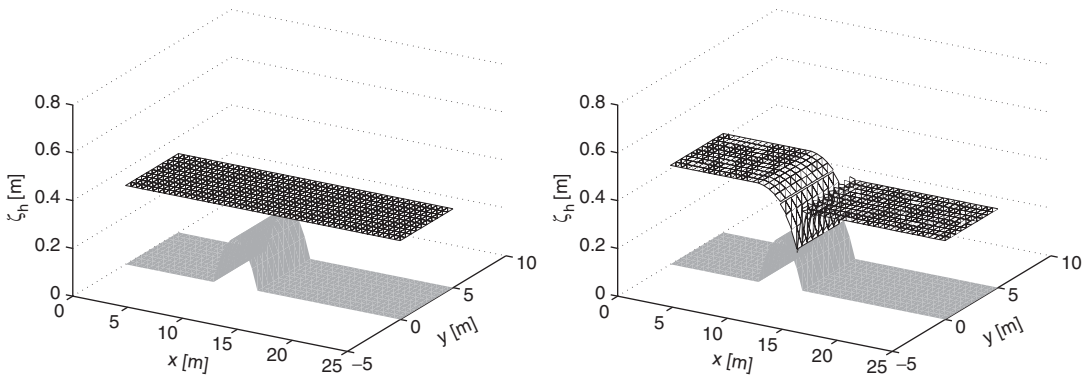

Figure 8. Transcritical flow with shock: initial (left) and final (right) approximate water heights for $p=1$.

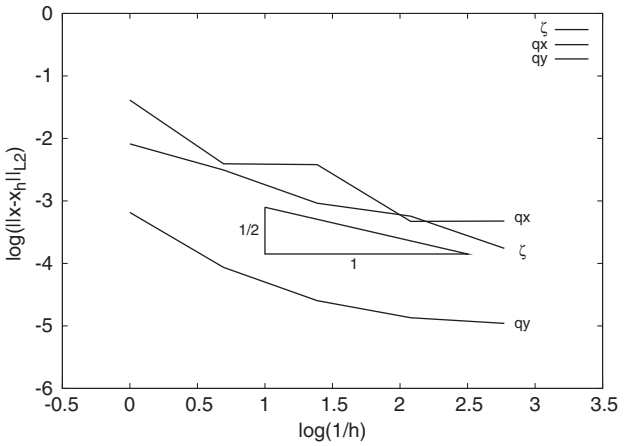

Figure 9. Transcritical flow with shock: L^2-errors on all the conservative variables ($p=1$).

Convergence towards the steady state was not fully achieved as the transient residual stopped decreasing after a typical time of $T=20\,\mathrm{s}$ (waves have traveled between the shock and the downwind boundary, but small time oscillations still take place near the shock). The so-called steady state presents a stationary shock (see Figure 8). For this case, the typical number of iterations is 5000, and the time step for $p=2$ is $\Delta t=0.0023\,\mathrm{s}$ for the finest mesh (for which $h=0.088\,\mathrm{m}$). The errors in the L^2-norm on all the conservative variables (water height and discharge) are illustrated in Figure 9 for $p=1$. As for reconstructed FV methods [8], the observed order of convergence is $\frac{1}{2}$.

5.3. *Flooding and drying*

5.3.1. Ritter solution [45]. We now study the capacity of the slope modification technique to treat flooding. The domain Ω is a $50\,\mathrm{m}\times 40\,\mathrm{m}$ rectangle and the bottom is flat. The initial discharge is

DOI: 10.1002/fld

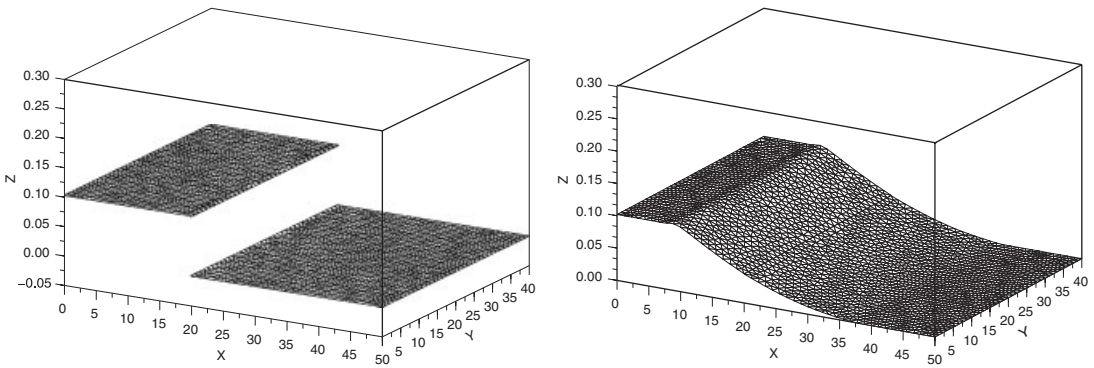

Figure 10. Rarefaction wave: initial (left) and final (right) approximate water heights for $p=1$.

$q=(0,0)\,\mathrm{m}^2/\mathrm{s}$ and the initial water height is set to zero for $x>20\,\mathrm{m}$ and to h_0 for $x<20\,\mathrm{m}$. The analytical solution is self-similar, i.e. it depends only on $\xi=(x-20)/t$. It is given by

$$\begin{aligned}
&\text{if } \xi<-\sqrt{gh_0}: && h(x,t)=h_0, && q(x,t)=0\\
&\text{else if } \xi>2\sqrt{gh_0}: && h(x,t)=0, && q(x,t)=0\\
&\text{else} && h(x,t)=\frac{1}{9g}(\xi-2\sqrt{gh_0})^2, && u(x,t)=\frac{2}{3}(\xi+\sqrt{gh_0})
\end{aligned}$$

We have taken h_0 such that $gh_0=1\,\mathrm{m}^2/\mathrm{s}^2$. The simulation time is $T=10\,\mathrm{s}$ (such that the rarefaction wave does not reach the boundary of the domain) and we consider unstructured meshes (however, meshes are fitted to the discontinuity in the initial solution). The threshold ε introduced in Section 4, for the slope modification technique is set to 10^{-6}. The initial and final approximate water heights are plotted for $p=1$ in Figure 10. For this case, the time step for $p=2$ is $\Delta t=0.0196\,\mathrm{s}$ for the finest mesh (for which $\mathfrak{h}=0.82\,\mathrm{m}$). The test case is solved starting with the analytical solution at time $t=2$. Thus the solution is at least everywhere continuous, but not continuously differentiable. The limiting process is not used since the solution is smooth enough. The errors in the L^2-norm on the water height are presented in Figure 11 for $p\in\{0,1,2\}$. The error on the water height behaves like $\mathfrak{h}^{0.8}$ for $p=0$ (an order of convergence between $\frac{1}{2}$ and 1 is expected), and, respectively, like $\mathfrak{h}^{1.3}$ and $\mathfrak{h}^{1.6}$ for $p=1$ and 2 (since the solution is not smooth at the left end of the rarefaction wave, the global accuracy should be limited to $\frac{3}{2}$). It is interesting to note that the error is localized in the regions where the solution is not very smooth (near both ends of the rarefaction fan), which means that the accuracy of the method in the present case is preserved far from relative singularities. This is shown by Figure 12 that represents the L^2-norm of the error on the water height in the region $\{x\in[15;35]\}$ at time $t=10\,\mathrm{s}$ for $p\in\{0,1,2\}$. One finds numerically that these errors behave, respectively, like $\mathfrak{h}^{0.8}$, $\mathfrak{h}^{2.5}$, and $\mathfrak{h}^{3.2}$ for $p\in\{0,1,2\}$.

5.3.2. Parabolic bowl. The aim is to assess the capacity of the method to treat flooding and drying. We consider a parabolic bowl (the ground corresponds to a paraboloid of revolution, i.e. $b(x,y)=\alpha r^2$ with $r^2=x^2+y^2$ and α is a positive constant) for which the exact solution has a periodic behavior and the free surface is an oscillating paraboloid of revolution. The analytical solution

DOI: 10.1002/fld

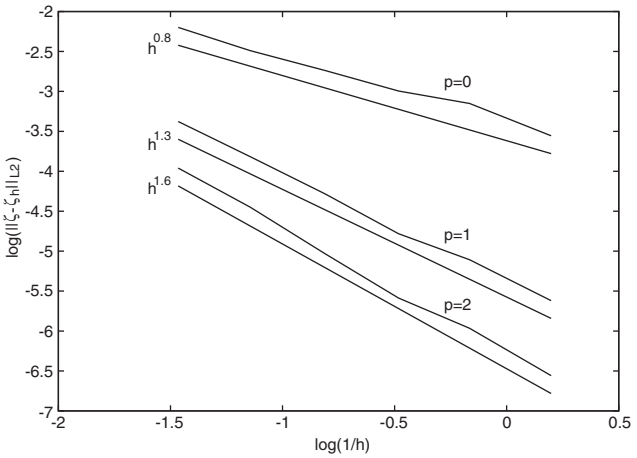

Figure 11. Rarefaction wave: overall L^2-error on the water height for $p \in \{0, 1, 2\}$.

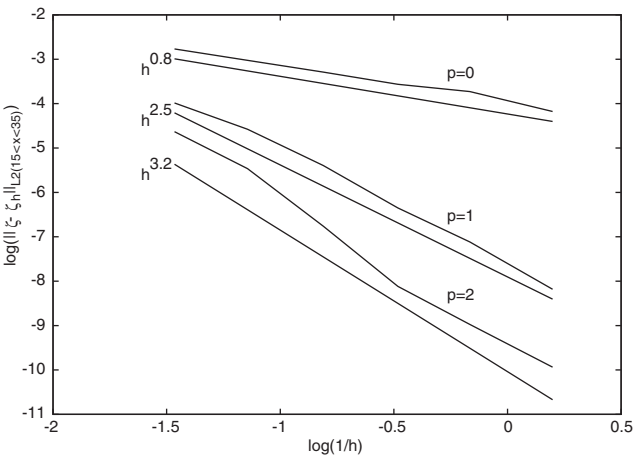

Figure 12. Rarefaction wave: local L^2-error over $\{x \in [15; 35]\}$ on the water height for $p \in \{0, 1, 2\}$.

(see [46] for more details) is such that $h(r, t)$ is nonzero for $r < \sqrt{(X + Y\cos\omega t)/\alpha(X^2 - Y^2)}$ (with $\omega^2 = 8g\alpha$, X and Y are constants such that $X > 0$ and $|Y| < X$), and

$$h(r,t) = \frac{1}{X + Y\cos\omega t} + \alpha(Y^2 - X^2)\frac{r^2}{(X + Y\cos\omega t)^2}$$

$$u(r,t) = -\frac{Y\omega\sin\omega t}{X + Y\cos\omega t}\left(\frac{x}{2}, \frac{y}{2}\right)^t \tag{28}$$

The solution is periodic with a period $\tau = 2\pi/\omega$. The computational domain Ω is a square of length $L = 8000\,\mathrm{m}$ centered at the origin. We set $\alpha = 1.6 \times 10^{-7}\,\mathrm{m}^{-1}$, $X = 1\,\mathrm{m}^{-1}$, and $Y = -0.41884\,\mathrm{m}^{-1}$. We use for this test case (with no relevant boundaries) a structured triangular mesh. The threshold

DOI: 10.1002/fld

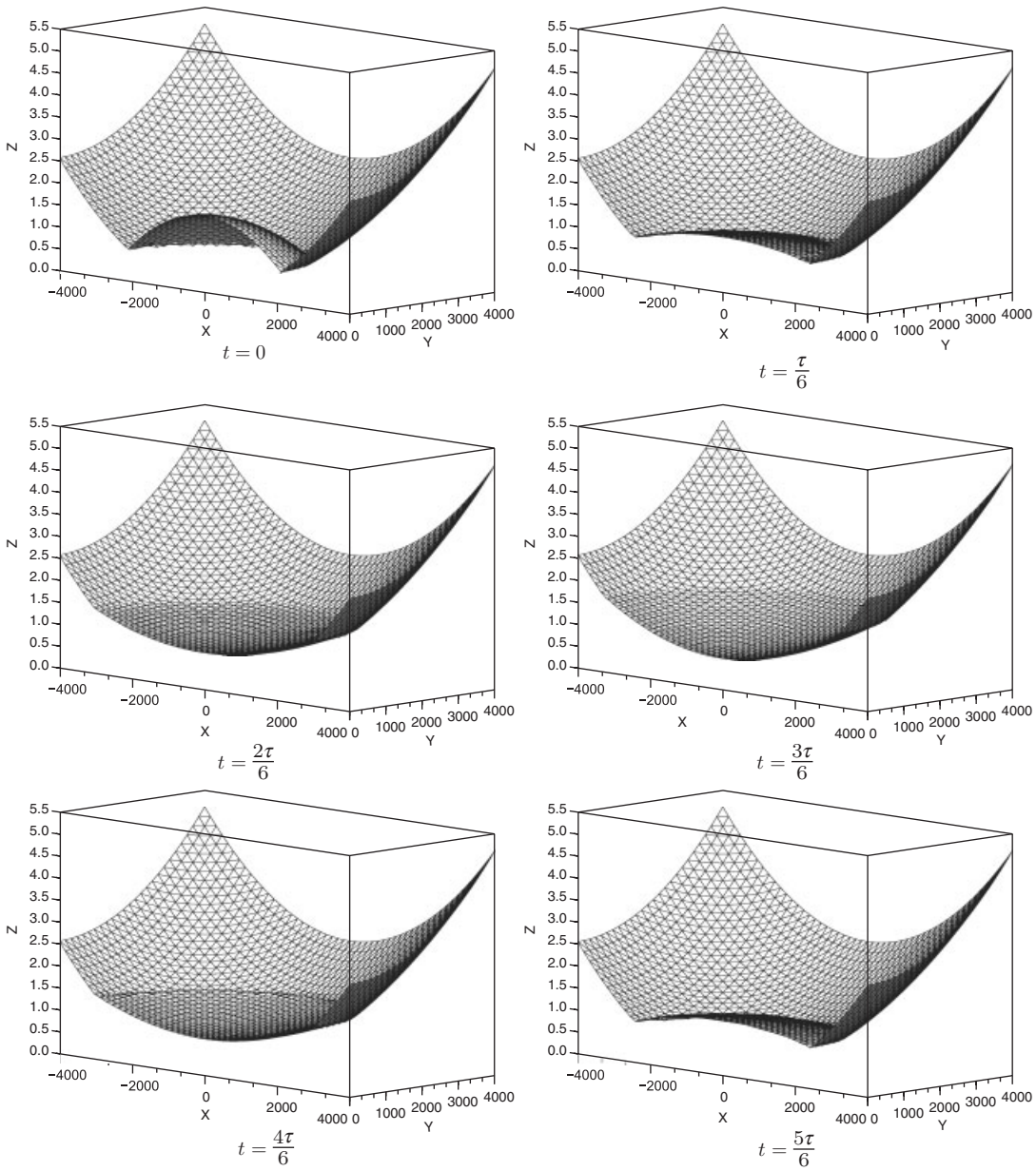

Figure 13. Parabolic bowl: approximate free surface elevation (i.e. $h_{\mathscr{D}} + b_{\mathscr{D}}$) for $p = 1$ at times $t = i(\tau/6)$, $(0 \leqslant i \leqslant 5)$.

DOI: 10.1002/fld

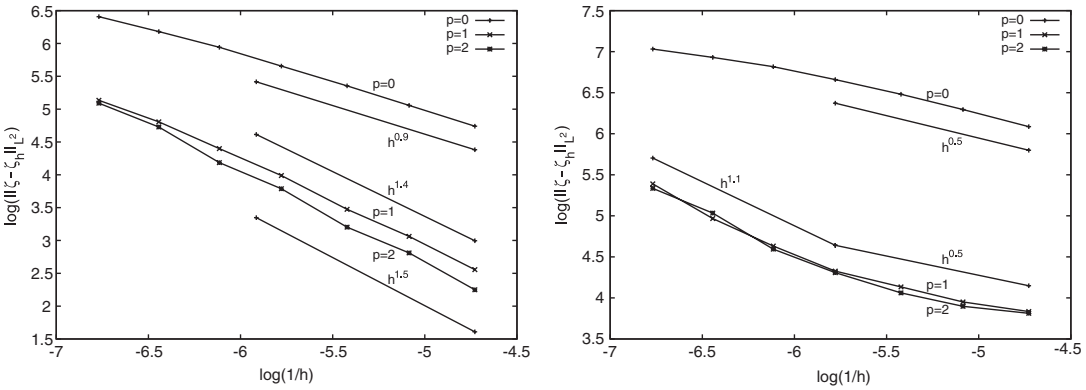

Figure 14. Parabolic bowl: for $p \in \{0, 1, 2\}$, $\max_{t \leqslant T}(\|h_{\mathscr{D}} - h\|_{L^2(\Omega)})$ for $T = \tau/2$ (left) and $T = \tau$ (right).

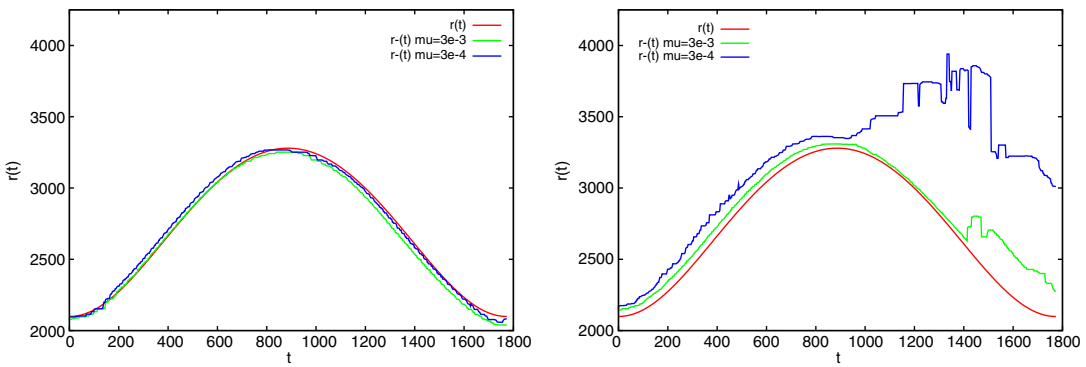

Figure 15. Parabolic bowl: $r^-(t, \mu)$ (left) and $r^+(t, \mu)$ (right) for $\mu = 10^{-2.5}$ and $10^{-3.5}$.

ε is set to 10^{-6}. We observe that the scale of this test case is close to realistic applications, the order of magnitude of the water height being around 2 m on a domain of kilometric size. For this case, the time step for $p = 2$ is $\Delta t = 1.61$ s for the finest mesh (for which $h = 113$ m).

The solution is illustrated at different times in Figure 13. It was obtained with $p = 1$ on a triangular mesh built by cutting rectangles of a 50×50 Cartesian mesh. The relative error in global mass conservation is less than 0.0002%, confirming that the average of $h_{\mathscr{D}}$ almost never takes negative values. The L^2-norm of the error on the water height is presented in Figure 14. Two different behaviors appear. During the first half-period ($t \in [0; \tau/2]$), the water spreads and flooding occurs. For $p = 0$, 1, and 2, the orders of convergence are, respectively, 0.9, 1.4, and 1.5. These results are close to the expected orders of convergence (respectively, 0.5, 1.5, and 1.5). However, for the second half-period ($t \in [\tau/2; \tau]$), the water flows back and drying occurs. For $p = 0$, the order of convergence is close to 0.5, while for $p = 1$ and 2, the orders of convergence are close to each other and vary from around 1.1 down to 0.5. This means that the drying algorithm does not perform as well as expected. One can remark that the flooding and drying algorithm plays the role of a limiter. In the flooding zones, it has to limit numerical oscillations due to high-order accuracy.

DOI: 10.1002/fld

However, in the drying zones, it has to limit both numerical oscillations and the physical drying process.

These two different behaviors can be illustrated by computing numerically the actual radius of the flooded zone during the computation. More precisely, we can compute (using the values of the discrete solution at quadrature points) the following radii:

- the exact radius of the flooded zone

$$r(t)=\sqrt{\frac{X+Y\cos\omega t}{\alpha(X^2-Y^2)}}$$

- for any threshold μ

$$r^-(t,\mu)=\min_{\{(x,y)/\,h_{\mathscr{D}}(t,x,y)\leqslant\mu\}}(\sqrt{x^2+y^2})$$

- for any threshold μ

$$r^+(t,\mu)=\max_{\{(x,y)/\,h_{\mathscr{D}}(t,x,y)>\mu\}}(\sqrt{x^2+y^2})$$

By definition, $r^-(t,\mu)\leqslant r^+(t,\mu)$ with equality for all μ if h is monotonically decreasing. Discrepancies between $r^-(t,\mu)$ and $r^+(t,\mu)$ indicate that h oscillates around the threshold μ. Furthermore, as $\mu\to 0$, $r^+(t,\mu)$ and $r^-(t,\mu)$ should be close to $r(t)$. In the zone $r<r^-(t,\mu)$, the ground can be considered as flooded (since $h_{\mathscr{D}}(t,x,y)>\mu$). On the contrary, in the zone $r>r^+(t,\mu)$, the ground can be considered as dry (since $h_{\mathscr{D}}(t,x,y)<\mu$). The zone $r^-(t,\mu)\leqslant r\leqslant r^+(t,\mu)$ is where the ground is marginally flooded. The different curves for $\mu\in\{10^{-2.5},10^{-3.5}\}$ are plotted in Figure 15 (polynomial order $p=1$, triangular mesh obtained by cutting rectangles of a 100×100 Cartesian mesh). The left part of Figure 15 shows that the flooded zone is quite accurately captured. The right part of the figure shows that the dry zone is not accurately captured during the drying phase (areas with small h are actually expanding during the computation for $\mu=10^{-3.5}$). In particular, observing $r^+(t,\mu=10^{-3.5})$ yields a possible explanation of accuracy loss in the drying phase of the computation: while zones with $h>10^{-3.5}$ remain limited during the flooding phase, they spread (or at least do not diminish) during the drying phase, where large areas with small h remain. Additional investigations on that specific behavior are under way. Anyway, one should keep in mind that these considerations are aimed at obtaining the sharpest possible asymptotic behavior for the numerical method, while spurious water heights below 1 mm are not a concern in practical simulations.

6. CONCLUSIONS

In this work, we have designed a well-balanced RKDG scheme for the SWE. In the absence of drying processes, the scheme performs well on structured or unstructured, fitted or unfitted meshes. As with classical CFE methods, the scheme delivers accurate solutions with high-order convergence rates whenever the solution is smooth enough. At the same time, the scheme can handle various nonsmooth wave structures (shocks, rarefaction fans) as FV methods. For drying processes, the scheme behaves satisfactorily in the present test case, since spurious oscillations

DOI: 10.1002/fld

where the water height takes small values can be controlled below 1 mm over a domain with kilometric scale. However, further investigations are needed in this direction.

APPENDIX A: THE HLLE AND HLLC FLUXES

Let $K \in \mathcal{T}_{\mathscr{D}}$, let $\sigma \in E^i_{\mathscr{D}}(K)$, and let K_σ be the element of $\mathcal{T}_{\mathscr{D}}$ sharing the interface σ with K. Let x_σ be an integration point on σ. Let $W_K = (h_K, u_K h_K)$ and $W_{K_\sigma} = (h_{K_\sigma}, u_{K_\sigma} h_{K_\sigma})$ be the two states on both sides of x_σ. Recall that $n_{K,\sigma}$ denotes the unit outward normal of K on σ.

The HLLE flux is used in one space dimension. This numerical flux is based on the approximation that the solution consists of three states, namely W_K, W_σ, and W_{K_σ}, separated by two waves of speeds $c_\sigma^\pm$. Letting $v_K = u_K \cdot n_{K,\sigma}$ and $v_{K_\sigma} = u_{K_\sigma} \cdot n_{K,\sigma}$ ($n_{K,\sigma} = \pm 1$), the wave speeds are evaluated as

$$c_\sigma^+ := \max(0, \max(v_{K_\sigma} + \sqrt{g h_{K_\sigma}}, v_\sigma^* + \sqrt{g h_\sigma^*}))$$

$$c_\sigma^- := \min(0, \min(v_K - \sqrt{g h_K}, v_\sigma^* - \sqrt{g h_\sigma^*}))$$

where

$$h_\sigma^* := \frac{h_K + h_{K_\sigma}}{2}, \quad v_\sigma^* := \frac{\sqrt{h_K} v_K + \sqrt{h_{K_\sigma}} v_{K_\sigma}}{\sqrt{h_K} + \sqrt{h_{K_\sigma}}}$$

are the so-called *Roe-averaged values*. Then, the HLLE flux is evaluated as

$$\phi_*^{\mathrm{HLLE}}(W_K, W_{K_\sigma}, n_{K,\sigma}) := \tfrac{1}{2}(\mathbb{F}_1(W_K) + \mathbb{F}_1(W_{K_\sigma})) n_{K,\sigma} + \tfrac{1}{2} Q_\sigma (W_K - W_{K_\sigma})$$

with

$$Q_\sigma := \frac{c_\sigma^+ + c_\sigma^-}{c_\sigma^+ - c_\sigma^-} \begin{pmatrix} 0 & 1 \\ -(v_\sigma^*)^2 + g h_\sigma^* & 2 v_\sigma^* \end{pmatrix} - 2 \frac{c_\sigma^+ c_\sigma^-}{c_\sigma^+ - c_\sigma^-} I_2$$

where I_2 is the identity matrix in $\mathbb{R}^{2,2}$.

In two space dimensions, the HLLC flux is preferred to the HLLE flux since the latter suffers from difficulties in resolving contact discontinuities and tangential waves. The HLLC flux is based on the approximation that the solution consists of four states, namely W_K, W_σ^-, W_σ^+, and W_{K_σ}, separated by three waves of speeds $c_\sigma^\pm$ and c_σ. The wave speeds are evaluated as

$$c_\sigma^- := \min(v_K - \sqrt{g h_K}, v_{K_\sigma} - \sqrt{g h_{K_\sigma}})$$

$$c_\sigma^+ := \max(v_K + \sqrt{g h_K}, v_{K_\sigma} + \sqrt{g h_{K_\sigma}})$$

$$c_\sigma := \frac{\frac{1}{2} g h_K^2 - \frac{1}{2} g h_{K_\sigma}^2 + h_{K_\sigma} v_{K_\sigma} (c_\sigma^+ - v_{K_\sigma}) - h_K v_K (c_\sigma^- - v_K)}{h_{K_\sigma} (c_\sigma^+ - v_{K_\sigma}) - h_K (c_\sigma^- - v_K)}$$

Then, the HLLC flux is evaluated as

$$\phi_*^{HLLC}(W_K, W_{K_\sigma}, n_{K,\sigma}) := \tfrac{1}{2}(\mathbb{F}_i(W_K) + \mathbb{F}_i(W_{K_\sigma})) n_{K,\sigma,i} + \tfrac{1}{2}((|c_\sigma^-| - |c_\sigma|) W_\sigma^- + (|c_\sigma^+| - |c_\sigma|) W_\sigma^+ + |c_\sigma^-| W_K + |c_\sigma^+| W_{K_\sigma})$$

DOI: 10.1002/fld

with

$$\frac{c_\sigma^- - c_\sigma}{c_\sigma^- - v_K} W_\sigma^- := W_K + \begin{pmatrix} 0 \\ h_K (c_\sigma - v_K) n_K \end{pmatrix}$$

and

$$\frac{c_\sigma^+ - c_\sigma}{c_\sigma^+ - v_{K_\sigma}} W_\sigma^+ := W_{K_\sigma} + \begin{pmatrix} 0 \\ h_{K_\sigma} (c_\sigma - v_{K_\sigma}) n_K \end{pmatrix}$$

ACKNOWLEDGEMENTS

This work was partly supported by the Direction de la Recherche et des Affaires Scientifiques et Techniques (DRAST) of the Ministère de l'équipement, des transports, de l'aménagement, du tourisme et de la mer under contract/grant number 04 DST 6 07. Fruitful discussions with Ph. Sergent and V. Laborie (CETMEF, France) are gratefully acknowledged. The authors are also thankful to the reviewers for their constructive comments that helped improve the article.

REFERENCES

1. Saint-Venant AJC. Théorie du mouvement non-permanent des eaux avec application aux crues des rivières et à l'introduction des marées dans leur lit. *Comptes Rendus de l'Academie des Sciences Paris* 1871; **73**:147–154.
2. Stoker JJ. *Water Waves*: *The Mathematical Theory with Applications*. Interscience Publishers: New York, 1957.
3. Vreugdenhil CB. *Numerical Methods for Shallow-Water Flow*. Kluwer Academic Publishers: Dordrecht, The Netherlands, 1994.
4. Godlewski E, Raviart P-A. Numerical approximation of hyperbolic systems of conservation laws. *Applied Mathematical Sciences*, vol. 118. Springer: New York, 1996.
5. Hervouet JM. Hydrodynamique des écoulements à surface libre, modélisation numérique avec la méthode des éléments finis. *Presses de l'École Nationale des Ponts et Chaussées*, 2003.
6. Katsaounis T, Makridakis C. Relaxation models and finite element schemes for the shallow water equations. *Hyperbolic Problems*: *Theory*, *Numerics*, *Applications*. Springer: Berlin, 2003; 621–631.
7. Zienkiewicz OC, Ortiz P. A split-characteristic based finite element model for the shallow water equations. *International Journal for Numerical Methods in Fluids* 1995; **20**:1061–1080.
8. Audusse E. Modélisation hyperbolique et analyse numérique pour les écoulements en eaux peu profondes. *Ph.D. Thesis*, Université de Paris VI, Paris, France, 2004.
9. Bermúdez A, Vázquez ME. Upwind methods for hyperbolic conservation laws with source terms. *Computers and Fluids* 1994; **23**:1049–1071.
10. Galloüet T, Hérard JM, Seguin N. Some approximate Godunov schemes to compute shallow-water equations with topography. *Computers and Fluids* 2003; **32**:479–513.
11. George DL. Numerical approximation of the nonlinear shallow-water equations with topography and dry beds. *Ph.D. Thesis*, University of Washington, WA, U.S.A., 2004.
12. Van Leer B. Towards the ultimate conservative difference scheme. II: Monotonicity and conservation combined in a second order scheme. *Journal of Computational Physics* 1974; **14**:361–370.
13. Liu X, Osher S, Chan T. Weighted essentially non-oscillatory schemes. *Journal of Computational Physics* 1994; **115**(1):200–212.
14. Lesaint P, Raviart P-A. On a finite element method for solving the neutron transport equation. *Mathematical Aspects of Finite Elements in Partial Differential Equations*. *Proceedings of the Symposium*, Mathematics Research Center, University of Wisconsin, Madison, WI, 1974. Academic Press: New York, Publication No. 33, 1974; 89–123.
15. Reed W, Hill T. Triangular mesh methods for the neutron transport equation. *Technical Report LA-UR-73-479*, Los Alamos, NM, Los Alamos Scientific Laboratory, 1973.

DOI: 10.1002/fld

16. Cockburn B, Shu CW. Runge–Kutta discontinuous Galerkin methods for convection-dominated problems. *Journal of Scientific Computing* 2001; **16**(3):173–261.
17. Cockburn B. Discontinuous Galerkin methods for convection-dominated problems. In *High-Order Methods for Computational Physics*, Barth T, Deconinck H (eds). Lecture Notes in Computational Science and Engineering, vol. 9. Springer: Berlin, 1999; 69–224.
18. Schwanenberg D, Köngeter J. A discontinuous Galerkin method for the shallow water equations with source terms. *Discontinuous Galerkin Methods*, Newport, RI, 1999. Lecture Notes in Computational Science and Engineering, vol. 11. Springer: Berlin, 2000; 419–424.
19. Li H, Liu R. The discontinuous Galerkin finite element method for the 2D shallow water equations. *Mathematics and Computers in Simulation* 2001; **56**(3):223–233.
20. Remacle J-F, Soares Frazão S, Li X, Shephard MS. An adaptive discretization of shallow-water equations based on discontinuous Galerkin methods. *International Journal for Numerical Methods in Fluids* 2006; **52**(8):903–923.
21. Eskilsson C, Sherwin SJ. A triangular spectral/*hp* discontinuous Galerkin method for modelling 2d shallow water equations. *International Journal for Numerical Methods in Fluids* 2004; **45**(6):605–623.
22. Bokhove O. Flooding and drying in discontinuous Galerkin finite-element discretizations of shallow-water equations. Part I: one dimension. *Journal of Scientific Computing* 2005; **22–23**:47–82.
23. Ambati VR, Bokhove O. Space–time discontinuous Galerkin finite element method for shallow water flows. *Journal of Computational and Applied Mathematics* 2006; **204**(2):452–462.
24. Tassi PA, Bokhove O, Vionnet CA. Space discontinuous Galerkin method for shallow water flows—kinetic and HLLC flux, and potential vorticity generation. *Advances in Water Resources* 2007; **30**(4):998–1015.
25. Aizinger V, Dawson C. A discontinuous Galerkin method for two-dimensional flow and transport in shallow water. *Advances in Water Resources* 2002; **25**:67–84.
26. Dawson C, Proft J. Coupled discontinuous and continuous Galerkin finite element methods for the depth-integrated shallow water equations. *Computer Methods in Applied Mechanics and Engineering* 2004; **193**(3–5):289–318.
27. Dawson C, Aizinger V. A discontinuous Galerkin method for three-dimensional shallow water equations. *Journal of Scientific Computing* 2005; **22/23**:245–267.
28. Giraldo FX, Hesthaven JS, Warburton T. Nodal high-order discontinuous Galerkin methods for the spherical shallow water equations. *Journal of Computational Physics* 2002; **181**(2):499–525.
29. Audusse E, Bouchut F, Bristeau M-O, Klein R, Perthame B. A fast and stable well-balanced scheme with hydrostatic reconstruction for shallow water flows. *SIAM Journal on Scientific Computing* 2004; **25**(6):2050–2065.
30. Xing Y, Shu CW. High order well-balanced finite volume WENO schemes and discontinuous Galerkin methods for a class of hyperbolic systems with source terms. *Journal of Computational Physics* 2006; **214**:567–598.
31. Brufau P, García-Navarro P, Vázquez-Cendón ME. A numerical model for the flooding and drying on irregular domains. *International Journal for Numerical Methods in Fluids* 2002; **39**:247–275.
32. Brufau P, García-Navarro P, Vázquez-Cendón ME. Zero mass error using unsteady wetting–drying conditions in shallow flows over dry topography. *International Journal for Numerical Methods in Fluids* 2004; **45**:1047–1082.
33. Schwanenberg D, Harms M. Discontinuous Galerkin finite-element method for transcritical two-dimensional shallow water flows. *Journal of Hydraulic Engineering* 2004; **130**(5):412–421.
34. Bunya S, Westerink J, Kubatko E, Dawson C. A new wetting and drying algorithm for discontinuous Galerkin solutions to the shallow water equations. *World Congress on Computational Mechanics*, vol. 7, Los Angeles, U.S.A., 2006.
35. Einfeldt B. On Godunov-type methods for gas dynamics. *SIAM Journal on Numerical Analysis* 1988; **25**(2): 294–318.
36. Einfeldt B, Munz CD, Roe PL, Sjögreen B. On Godunov-type methods near low densities. *Journal of Computational Physics* 1991; **92**:273–295.
37. Bristeau MO, Coussin B. Boundary conditions for the shallow-water equations solved by kinetic schemes. *Technical Report RR-4282*, INRIA, 2001.
38. Piperno S. Symplectic local time-stepping in non-dissipative DGTD methods applied to wave propagation problems. *M2AN Mathematical Modelling and Numerical Analysis* 2006; **40**(5):815–841.
39. Chauviere C, Hesthaven J, Kanevsky A, Warburton T. High-order localized time integration for grid-induced stiffness. *Proceedings of the Second MIT Conference on Computational Fluid and Solid Mechanics,* MIT, Cambridge, MA, U.S.A., 17–20 June 2003.
40. Krivodonova L, Xin J, Remacle JF, Chevaugeon N, Flaherty JE. Shock detection and limiting with discontinuous Galerkin methods for hyperbolic conservation laws. *Journal of Computational Physics* 2004; **48**:323–338.
41. Noelle S, Pankratz N, Puppo G, Natvig JR. Well-balanced finite volume schemes of arbitrary order of accuracy for shallow water flows. *Journal of Computational Physics* 2006; **213**:474–499.

DOI: 10.1002/fld

42. Chen G, Liu J. Convergence of second-order schemes for isentropic gas dynamics. *Mathematics of Computation* 1993; **61**(204):607–627.
43. Alcrudo F, Garcia-Navarro P. A high-resolution Godunov-type scheme in finite volumes for the 2d shallow-water equations. *International Journal for Numerical Methods in Fluids* 1993; **16**:489–505.
44. Goutal N, Maurel F. Proceeding of the second workshop on dam-break simulation. *Technical Report HE-43/97/016/B, EDF*, 1997.
45. Ritter A. Die Fortpflanzung der Wasserwellen. *Vereine Deutscher Ingenieure Zeitschrift* 1892; **36**(2):947–954.
46. Thacker WC. Some exact solutions to the nonlinear shallow-water wave equations. *Journal of Fluid Mechanics* 1981; **107**:499–508.

DOI: 10.1002/fld